HHS Public Access

Author manuscript

J Biomech. Author manuscript; available in PMC 2017 October 03.

Published in final edited form as:

J Biomech. 2016 October 3; 49(14): 3549–3554. doi:10.1016/j.jbiomech.2016.08.018.

A Pediatric Animal Model to Evaluate the Effects of Disuse on Musculoskeletal Growth and Development

Daniel L Miranda[1], **Melissa Putman**[2], **Ruby Kandah**[1], **Maria Cubria**[3], **Sebastian Suarez**[3], **Ara Nazarian**[3], and **Brian Snyder**[3,4]

[1]Wyss Institute for Biologically Inspired Engineering at Harvard University, Boston, MA

[2]Division of Endocrinology, Boston Children's Hospital and Harvard Medical School, Boston, MA

[3]Center for Advanced Orthopaedic Studies, Beth Israel Deaconess Medical Center and Harvard Medical School, Boston, MA

[4]Department of Orthopedic Surgery, Boston Children's Hospital and Harvard Medical School, Boston, MA

Abstract

Prolonged immobilization in hospitalized children can lead to fragility fractures and muscle contractures and atrophy. The purpose of this study was to develop a lower-extremity disuse rabbit model with musculoskeletal changes similar to those observed in children subjected to prolonged immobilization. Six-week-old rabbits were randomly assigned to control (CTRL, n=4) or bilateral sciatic and femoral neurectomy (bSFN, n=4) groups. Trans-axial helical CT scans of each rabbit's hind limbs were acquired after eight weeks. The rabbits were then euthanized and the tibiae and calcanea were harvested from each rabbit. μCT imaging was performed on the tibiae and calcanea mid-diaphysis. Four-point bending, gas pycnometry, and ashing were then performed on each tibia. All comparisons reflect the differences between the bSFN and CTRL rabbits. Significant decreases in tibiae bone mineral density (≥9.41%, $p \leq 0.006$), axial rigidity (≥50.47%, $p \leq 0.02$), and soft tissue mass (55.25%, $p = 0.006$) were observed from the trans-axial helical CT scans. The μCT results indicated significant detriments in tibia and calcaneus cortical thickness and bone volume fraction ($p \leq 0.011$). Significant changes in stiffness, yield load, ultimate load, and ultimate displacement (≥30.05%, $p \leq 0.025$) were observed from mechanical testing. These data indicate that limb disuse at a time of rapid musculoskeletal growth severely impairs muscle and bone development, reflecting the musculoskeletal complications observed in children with chronic medical conditions causing immobilization. Interventions to reduce these musculoskeletal complications in children are urgently needed. This disuse rabbit model will be useful in pre-clinical studies evaluating novel interventions for improving pediatric musculoskeletal health.

Corresponding Author: Daniel L Miranda, 3 Blackfan Circle, 2nd Floor, Room 208, Boston, MA 02115, Telephone: (970) 581-8040, Fax: (617) 432-8252, daniel.miranda@wyss.harvard.edu.
Daniel L Miranda (co-first author), Melissa Putman (co-first author)

Conflict of interest statement

The authors have no financial or personal relationships that could bias this work.

Keywords

neurectomy; bone; density; geometry; muscle; cross-section; rabbit

1. Introduction

Medical treatments and disease pathophysiology can result in prolonged immobilization that places hospitalized and chronically ill infants and children at risk for serious secondary complications including fragility fractures (Huh and Gordon, 2013), muscle contractures and atrophy (Boonyarom and Inui, 2006). This is due to immobilization-induced bone loss and impairment of muscle function secondary to reduced levels of activity or limb disuse (Boonyarom and Inui, 2006; Ward et al., 2004). Pediatric patients at the highest risk for inpatient fracture include premature infants (Huh and Gordon, 2013; Moyer-Mileur et al., 2000) and children with cerebral palsy (Caulton et al., 2004; Mergler et al., 2009), spinal cord injury (Munns and Cowell, 2005; Ward et al., 2004), neuromuscular disorders such as Duchenne Muscular Dystrophy (Ward et al., 2004) or Spinal Muscular Atrophy (Rudnik-Schöneborn et al., 2008), prolonged post-operative immobilization such as esophageal atresia (Bairdain et al., 2014; Huh and Gordon, 2013), and prolonged dependence on parenteral nutrition (Diamanti et al., 2010). Despite the institution of fracture precautions, optimization of parenteral nutrition and vitamin D intake, and regular physical therapy, these patients continue to suffer from high rates of fracture during hospitalization (Bairdain et al., 2014; Huh and Gordon, 2013; Moyer-Mileur et al., 2000). Therefore, other approaches must be pursued to optimize musculoskeletal health and reduce fracture rates in hospitalized infants.

Muscle atrophy, osteoporosis, and fragility fractures have long been a major concern in the elderly (Johnell and Kanis, 2006), and several animal models have been developed to portray disuse atrophy, osteopenia, and fragility fractures in adults (Egermann et al., 2005). However, there are no pediatric models available that incorporate immature and developing large animals (e.g., rabbits). A large animal model is required to specifically test interventions to address musculoskeletal complications arising from disuse and lack of weight bearing seen in a variety of pediatric inpatients (Huh and Gordon, 2013). Neurectomy is a promising technique that has been used in the past to model musculoskeletal disuse (Komori, 2015). However, these studies have typically focused on a single nerve ligation that leaves substantial hindlimb musculature intact. Additionally, these studies have been limited to fully-grown small animals, such as mice and rats (Brouwers et al., 2009; Feng et al., 2016; Komori, 2015; Sugiyama et al., 2012). Therefore, the purpose of this study was to develop a pediatric lower-extremity disuse rabbit model. We hypothesize that bilateral sciatic and femoral neurectomies in six-week-old rabbits will affect bone and muscle development in the lower extremity similar to the musculoskeletal changes observed in children who are sedated and/or muscle relaxed with paralytics such as vecuronium during their hospitalization.

2. Methods

2.1. Animals

The Beth Israel Deaconess Medical Center Institutional Animal Care and Use Committee approved all experimental procedures used for this study. Female New Zealand white rabbits were chosen, due to their docile and non-aggressive nature, making them easy to handle and observe. Furthermore, the rabbit's skeletal size and bone density is similar to human infants, and skeletal growth is completed by 28 weeks. This allows research to be conducted during the growth phase in a reasonable time period.

2.2. Surgical Procedures

Six-week-old rabbits were randomly assigned to either control (CTRL, n=4) or bilateral sciatic and femoral neurectomy (bSFN, n=4) groups. The rabbits in the CTRL group did not undergo any intervention. Rabbits undergoing surgical bSFN were anesthetized with intramuscular doses of Ketamine (35 mg/kg) and Xylazine (2.5 mg/kg) and then maintained on 1–2% isoflurane delivered through a mask. The fur was shaved and skin wiped with betadine and alcohol.

After administering anesthesia, each bSFN rabbit was placed in the prone position with the posterior limbs mildly rotated externally with semiflexion of the knees. An oblique incision distal the posterior superior iliac spine was deepened to expose the Gluteus Maximus muscle, which was split by blunt dissection, and the sciatic nerve was identified on top of the piriformis muscle exiting the sciatic notch. Before the nerve was sharply bisected, a small amount (approximately 1–2 ml) of phenol was applied directly onto the nerve to cause chemical demyelination to prevent nerve regeneration and reduce the incidence of autotomy. The notch was then over-sewn with a nylon suture, and the operative incision was closed in a hidden subcuticular pattern with absorbable sutures. These procedures were performed for the left and right sciatic nerves following established techniques (Bradley et al., 1998; Jiang et al., 2006; Sames and Benes, 1997; Sung, 2004).

Each bSFN rabbit was then placed in the supine position to perform bilateral femoral neurectomy. Through an incision just distal to the inguinal ligament, the femoral nerve was identified and mobilized in the femoral triangle medial to the Sartorius muscle. The femoral artery and vein were carefully retracted. Neurectomy was performed by chemical neurolysis using phenol prior to bisecting it with electrocautery. These procedures were performed for the left and right sciatic nerves following established techniques (Hanashi et al., 2002; O'Connor et al., 1992; Sung, 2004). The combined bSFN procedure resulted in hind limb disuse, while allowing the rabbit to move independently using its forelimbs and to eat, void, and defecate spontaneously.

2.3. Study Procedures

Both CTRL and bSFN groups were housed with their lactating mothers for eight weeks after the surgical procedures. The surgical procedures resulted in the bSFN rabbits having limited activity and reduced mobility. The rabbits were moved, cleaned, and bedding was changed regularly to avoid pressure sores and urine scald. Additionally, monitoring the rabbit's hind

limbs daily and bandaging when appropriate mitigated digit autotomy. The rabbits gained weight as expected on a standard rabbit chow diet supplemented with DietGel Criticare (ClearH_2O, Portland, ME, USA) as needed. After eight weeks, the rabbits were anesthetized through intramuscular doses of Ketamine and Xylazine and euthanized by a fatal dose of Fatal-Plus (0.22 ml/kg).

2.3.1. Clinical CT scans—Trans-axial helical CT scans (0.2 mm^3 voxel size, 120 kVp tube voltage, 300 mA tube current) of each rabbit's hind limbs were acquired (Aquilon 64, Toshiba, Tustin, CA, USA) eight weeks post-surgery. Three hydroxyapatite phantoms of known mineral density (0, 500, and 1000 mgHA/cm^3) were used to convert Hounsfield units (HU) to volumetric bone mineral density (vBMD). Segmented CT images of the left tibia were reformatted (Mimics v16; Materialise, Ann Arbor, MI, USA) to generate transaxial images perpendicular to the anatomical axis. Axial rigidity was derived for every cross-section using CT-based Rigidity Analysis (CTRA) to calculate the integral of the modulus weighted pixels distributed in space over the cross-sectional profile of bone (Gordon et al., 2011; Villa-Camacho et al., 2014; Whealan et al., 2000). The vBMD and axial rigidity were then extracted from the five axial slices surrounding the 4%, 38%, and 66% of the total length measured from the distal end (Figure 1). These sites were chosen because they represent standard clinical peripheral quantitative CT sites used in children and adolescents (Adams et al., 2014). The soft tissue mass, normalized by body weight, was also calculated from the volume and density of the five axial slices surrounding the 38% total tibia length site. This location was chosen because the gastrocnemius muscle diameter in healthy control rabbits was the greatest at this site. Each rabbit's hind limbs were harvested after the clinical CT scan, and the tibiae and calcanea were dissected and stripped of soft tissue. Each bone was wrapped in gauze soaked in 0.9% saline and stored at −20 °C.

2.3.2. μCT scans—Prior to imaging, the tibiae were thawed out at room temperature and re-hydrated in 0.9% saline for 30 minutes. The proximal and distal epiphyses of each bone were then cut using two parallel diamond wafering blades on a low-speed saw (Isomet, Buehler Corporation, Lake Bluff, Illinois) under copious irrigation. Micro-computed tomography (μCT) imaging (μCT 40, Scanco Medical AG, Brüttisellen, Switzerland) was performed on tibial and calcaneal mid-diaphysis sections (100 slices, 30 μm isotropic voxel size, 250 ms integration time, 55 kV tube voltage, 145 mA tube current) to derive cortical thickness (Ct.Th) and bone area fraction (BA/TA). Hydroxyapatite phantoms of known mineral density (0, 100, 200, 400, and 800 mgHA/cm^3) were used to convert attenuation coefficients to vBMD.

2.3.3. Mechanical Testing—Four-point bending was performed on tibias using an Instron 8511 (Instron, Norwood, MA, USA) load frame under displacement control with 50 mm support and 20 mm loading spans (Figure 2). Specimens were thawed out to room temperature and re-hydrated in 0.9% for 30 minutes prior to testing. The posterior surface of the tibiae were placed facing upward on the support span and lightly secured with elastic bands to avoid rolling during testing. The loading crosshead was mounted on a pivot in order to ensure symmetrical loading of the irregularly shaped rabbit tibiae at all four loading points. Each tibia was loaded to failure at a constant rate of 0.1 mm/s. Modulus of elasticity,

yield load, ultimate load, ultimate displacement, ultimate stress, and flexural modulus were calculated using standard composite beam equations in MATLAB (MathWorks, Natick, MA, USA).

2.3.4. Helium Pycnometry and Ashing—Eight-millimeter long bone segments, adjacent to the fracture site, were excised after mechanical testing, in order to assess the following true bone tissue parameters: wet and dry bone densities, mineral and matrix densities, and mineral and matrix content. Helium pycnometry is a useful technique to calculate the true density of a solid material, with an unknown volume but a known weight. The pycnometer allows helium to enter the chamber where the sample is placed, and calculates the average volume of the sample as the space from which the gas is excluded.

Each bone segment was weighed three times using an Analytical Plus Electronic Balance (AP210s; Ohaus Corporation, Florham Park, NJ, USA), scale readings were recorded, and mean values were calculated. The volume from each bone segment was determined using a pycnometer (Accupyc 1330; Micromeritics, Norcross, GA, USA). In order to guarantee reproducibility and fidelity to the results, the gas pycnometer was working under a controlled temperature of 26±1 °C. Wet bone density was then calculated.

Specimens were then placed in a labeled container and dehydrated at 75 °C for 72 hours in a Thermolyne Furnace Type 48000 (Barnstead International, Dubuque, Iowa, USA) and weighed at 12-hour intervals until no changes in weight were recorded. The final mass measurements after dehydration were used to calculate dry bone density. Specimens were ashed at 600°C for 12 additional hours and were allowed to cool for one hour with the furnace door open. A final mass measurement was performed, and mineral and matrix densities and content were calculated (Carter et al., 1981)

2.4. Statistical Analysis

The Kolmogorov-Smirnov goodness of fit test was used to assess distribution normality. A one-tailed unpaired Student’s t-test was used to test for differences between the CTRL and bSFN groups for each of the outcome measures described. A one-tailed test was chosen based on the a-priori hypothesis that bSFN would either have no effect or degrade bone quality and soft tissue mass.

3. Results

Using clinical CT, significant decreases in the tibiae vBMD and axial rigidity were observed eight weeks after the surgical procedures. At the 4%, 38%, and 66% cross-sections, the average tibiae cortical bone vBMD was 9.81% (p=0.004), 10.18% (p=0.004), 9.41% (p=0.006) lower for the bSFN group compared to the CTRL group. At the same cross-sections, the corresponding tibiae axial rigidities were 67.56% (p=0.006), 50.92% (p = 0.011), and 50.47% (p=0.020) less for the bSFN group compared to the CTRL group. The soft tissue envelope surrounding the 38% cross-section was 55.28% (p=0.006) less for the bSFN group compared to the CTRL group.

On μCT testing, cortical thickness and bone area fraction were 31.04% (p=0.005) and 11.92% (p=0.056) less for the bSFN rabbits compared to the CTRL rabbits, respectively (Figure 3). Calcaneal Ct.Th and BA/TA were 53.20% (p<0.001) and 1.61% (p=0.011) less for the bSFN rabbits compared to the CTRL rabbits, respectively (Figure 3).

Mechanical testing (Figure 4) indicated significant reductions in stiffness (52.25% lower, p<0.001), yield load (41.82% lower, p<0.001), ultimate load (39.01% lower, p=0.001), and an increase in ultimate displacement (30.05% higher, p=0.025).

Matrix density (p = 0.042) was the only true bone tissue outcome where the bSFN group had a significant decrease compared to the CTRL group (Figure 5).

4. Discussion

The goal of this study was to develop a disuse rabbit model by performing bilateral sciatic and femoral neurectomies in six-week-old rabbits with the hypothesis that it would result in marked decreases in the bone and muscle development of the lower extremity. Overall, the data indicate that limb disuse at a time of rapid growth of the musculoskeletal system severely impairs both muscle and bone development.

Structural and material property indices measured *in-vivo* from helical CT images and *ex-vivo* by μCT and mechanical testing show that bone and muscle properties decrease, as reflected by a decrement in the cross-sectional bone geometry and reduction in the bone tissue material properties related to diminution in vBMD. The lack of difference in the true bone tissue outcomes between the groups, combined with a decline in vBMD, implicates under mineralization of the bone tissue, an observation further supported mechanically by the increase in ultimate displacement. Importantly, the predicted changes in bone structure and function calculated from the analysis of non-invasive *in-vivo* helical CT images were confirmed by mechanical testing and compositional analysis of post-mortem specimens.

Interventions to reduce the musculoskeletal complications of limb disuse and/or immobilization in infants and children are urgently needed. For example, episodes of musculoskeletal disuse from sedation appear to be the most significant risk factor for fractures in pediatric patients who underwent treatment for Long-Gap Esophageal Atresia (Bairdain et al., 2015). Fracture rates of up to 40% were observed in these patients, and clinically they show evidence of increased bone resorption and decreased bone formation attributed to their prolonged immobilization. In general, disease pathophysiology, medical treatments, nutritional status, and immobilization are all considered risk factors for fragility fractures in hospitalized children (Huh and Gordon, 2013). It is critical to develop novel treatments to prevent morbidity associated with fractures and to optimize immediate and future bone health in these at-risk patients. This pediatric paralytic rabbit model will be useful for understanding the role of normal muscle function and fluid flow on modulating musculoskeletal growth. Additionally, this model will permit pre-clinical tests of innovative treatments that ameliorate bone resorption and muscle atrophy in afflicted children. Moreover, the bone structural indices calculated from *in-vivo* helical CT images were

sensitive enough to effectively and non-invasively quantify changes in bone function, allowing for *in-vivo* evaluations of the rabbits as well as human clinical populations.

Limitations of this study include the small number of rabbits studied; however, the observed striking differences in bone and muscle outcomes suggest that the study was sufficiently powered. Additionally, no sham surgeries were performed in the CTRL group. Young rabbits are notoriously fragile and pain sensitive. We sought to avoid subjecting additional rabbits to the risks of, complications from, and pain associated with the surgical procedures. Finally, due to the paucity of trabecular bone present in rabbit tibiae and calcanei, specific changes in trabecular bone could not be assessed. However, we can infer from the observed cortical bone loss that significant trabecular loss also likely occurred (Parfitt, 1983) based on studies evaluating disuse-associated bone loss in other animal models (Jiang et al., 2007; LeBlanc et al., 1985; Liu et al., 2008; Yarrow et al., 2014).

In conclusion, bSFN in young rabbits leads to reductions in bone density, structure, and strength, and a decrease in muscle mass that reflect the musculoskeletal complications observed in infants and children with chronic medical conditions causing immobilization. This disuse rabbit model will be useful in pre-clinical studies evaluating interventions for improving musculoskeletal health in immobilized pediatric patients.

Supplementary Material

Refer to Web version on PubMed Central for supplementary material.

Acknowledgments

This work was supported by Center for Musculoskeletal Research Pilot Grant (1P30AR066261-01), Thrasher Research Fund Early Career Award, Boston Children's Hospital Innovestment Award, the NIH LRP (AN and MSP) and the Wyss Institute.

References

Adams JE, Engelke K, Zemel BS, Ward KA. International Society of Clinical Densitometry. Quantitative computer tomography in children and adolescents: the 2013 ISCD Pediatric Official Positions. J Clin Densitom. 2014

Bairdain S, Dodson B, Zurakowski D, Rhein L, Snyder BD, Putman M, Jennings RW. High incidence of fracture events in patients with Long-Gap Esophageal Atresia (LGEA): A retrospective review prompting implementation of standardized protocol. Bone Reports. 2015; 3:1–4.

Bairdain S, Kelly DP, Tan C, Dodson B, Zurakowski D, Zurakowksi D, Jennings RW, Trenor CC. High incidence of catheter-associated venous thromboembolic events in patients with long gap esophageal atresia treated with the Foker process. J. Pediatr. Surg. 2014; 49:370–373. [PubMed: 24528989]

Boonyarom O, Inui K. Atrophy and hypertrophy of skeletal muscles: structural and functional aspects. Acta Physiol (Oxf). 2006; 188:77–89. [PubMed: 16948795]

Bradley JL, Abernethy DA, King RH, Muddle JR, Thomas PK. Neural architecture in transected rabbit sciatic nerve after prolonged nonreinnervation. J. Anat. 1998; 192(Pt 4):529–538. [PubMed: 9723980]

Brouwers JEM, Lambers FM, van Rietbergen B, Ito K, Huiskes R. Comparison of bone loss induced by ovariectomy and neurectomy in rats analyzed by in vivo micro-CT. J. Orthop. Res. 2009; 27:1521–1527. [PubMed: 19437511]

Carter DR, Caler WE, Spengler DM, Frankel VH. Uniaxial fatigue of human cortical bone. The influence of tissue physical characteristics. J Biomech. 1981; 14:461–470. [PubMed: 7276007]

Caulton JM, Ward KA, Alsop CW, Dunn G, Adams JE, Mughal MZ. A randomised controlled trial of standing programme on bone mineral density in non-ambulant children with cerebral palsy. Arch. Dis. Child. 2004; 89:131–135. [PubMed: 14736627]

Diamanti A, Bizzarri C, Bizzarri C, Basso MS, Gambarara M, Cappa M, Daniele A, Noto C, Castro M. How does long-term parenteral nutrition impact the bone mineral status of children with intestinal failure? J. Bone Miner. Metab. 2010; 28:351–358. [PubMed: 20033239]

Egermann M, Goldhahn J, Schneider E. Animal models for fracture treatment in osteoporosis. Osteoporos Int. 2005; 16:S129–S138. [PubMed: 15750681]

Feng BO, Wu W, Wang H, Wang J, Huang D, Cheng L. Interaction between muscle and bone, and improving the effects of electrical muscle stimulation on amyotrophy and bone loss in a denervation rat model via sciatic neurectomy. Biomed Rep. 2016; 4:589–594. [PubMed: 27123252]

Gordon CM, Gordon LB, Snyder BD, Nazarian A, Quinn N, Huh SY, Giobbie Hurder A, Neuberg D, Cleveland R, Kleinman M, Miller DT, Kieran MW. Hutchinson-Gilford progeria is a skeletal dysplasia. J. Bone Miner. Res. 2011; 26:1670–1679. [PubMed: 21445982]

Hanashi D, Koshino T, Uesugi M, Saito T. Effect of femoral nerve resection on progression of cartilage degeneration induced by anterior cruciate ligament transection in rabbits. J Orthop Sci. 2002; 7:672–676. [PubMed: 12486471]

Huh SY, Gordon CM. Fractures in hospitalized children. Metab. Clin. Exp. 2013; 62:315–325. [PubMed: 22959479]

Jiang S-D, Jiang L-S, Dai L-Y. Changes in bone mass, bone structure, bone biomechanical properties, and bone metabolism after spinal cord injury: a 6-month longitudinal study in growing rats. Calcif. Tissue Int. 2007; 80:167–175. [PubMed: 17340221]

Jiang S-D, Jiang L-S, Dai L-Y. Spinal cord injury causes more damage to bone mass, bone structure, biomechanical properties and bone metabolism than sciatic neurectomy in young rats. Osteoporos Int. 2006; 17:1552–1561. [PubMed: 16874443]

Johnell O, Kanis JA. An estimate of the worldwide prevalence and disability associated with osteoporotic fractures. Osteoporos Int. 2006; 17:1726–1733. [PubMed: 16983459]

Komori T. Animal models for osteoporosis. Eur. J. Pharmacol. 2015; 759:287–294. [PubMed: 25814262]

LeBlanc A, Marsh C, Evans H, Johnson P, Schneider V, Jhingran S. Bone and muscle atrophy with suspension of the rat. J. Appl. Physiol. 1985; 58:1669–1675. [PubMed: 3158639]

Liu D, Zhao C-Q, Li H, Jiang S-D, Jiang L-S, Dai L-Y. Effects of spinal cord injury and hindlimb immobilization on sublesional and supralesional bones in young growing rats. Bone. 2008; 43:119–125. [PubMed: 18482879]

Mergler S, Evenhuis HM, Boot AM, De Man SA, Bindels-De Heus KGCB, Huijbers WAR, Penning C. Epidemiology of low bone mineral density and fractures in children with severe cerebral palsy: a systematic review. Dev Med Child Neurol. 2009; 51:773–778. [PubMed: 19614941]

Moyer-Mileur LJ, Brunstetter V, McNaught TP, Gill G, Chan GM. Daily physical activity program increases bone mineralization and growth in preterm very low birth weight infants. Pediatrics. 2000; 106:1088–1092. [PubMed: 11061779]

Munns CF, Cowell CT. Prevention and treatment of osteoporosis in chronically ill children. J Musculoskelet Neuronal Interact. 2005; 5:262–272. [PubMed: 16172517]

O'Connor BL, Visco DM, Brandt KD, Myers SL, Kalasinski LA. Neurogenic acceleration of osteoarthrosis. The effects of previous neurectomy of the articular nerves on the development of osteoarthrosis after transection of the anterior cruciate ligament in dogs. J Bone Joint Surg Am. 1992; 74:367–376. [PubMed: 1548263]

Parfitt, AM. Bone Histomorphometry. In: Recker, RR., editor. Techniques and Interpretation. CRC; 1983. p. 143-223.

Rudnik-Schöneborn S, Heller R, Berg C, Betzler C, Grimm T, Eggermann T, Eggermann K, Wirth R, Wirth B, Zerres K. Congenital heart disease is a feature of severe infantile spinal muscular atrophy. J. Med. Genet. 2008; 45:635–638. [PubMed: 18662980]

Sames M, Benes V. Surgical approach to the rabbit sciatic nerve. Technical note. Acta Chir Plast. 1997; 39:65–67. [PubMed: 9294910]

Sugiyama T, Meakin LB, Browne WJ, Galea GL, Price JS, Lanyon LE. Bones' adaptive response to mechanical loading is essentially linear between the low strains associated with disuse and the high strains associated with the lamellar/woven bone transition. Journal of Bone and Mineral Research. 2012; 27:1784–1793. [PubMed: 22431329]

Sung DH. Locating the target nerve and injectate spread in rabbit sciatic nerve block. Reg Anesth Pain Med. 2004; 29:194–200. [PubMed: 15138902]

Villa-Camacho JC, Iyoha-Bello O, Behrouzi S, Snyder BD, Nazarian A. Computed tomography-based rigidity analysis: a review of the approach in preclinical and clinical studies. BoneKEy Reports. 2014; 3:587. [PubMed: 25396051]

Ward K, Alsop C, Caulton J, Rubin CT, Adams J, Mughal Z. Low magnitude mechanical loading is osteogenic in children with disabling conditions. J. Bone Miner. Res. 2004; 19:360–369. [PubMed: 15040823]

Whealan KM, Kwak SD, Tedrow JR, Inoue K, Snyder BD. Noninvasive Imaging Predicts Failure Load of the Spine with Simulated Osteolytic Defects*†. J Bone Joint Surg Am. 2000; 82:1240–1240. [PubMed: 11005515]

Yarrow JF, Ye F, Balaez A, Mantione JM, Otzel DM, Chen C, Beggs LA, Baligand C, Keener JE, Lim W, Vohra RS, Batra A, Borst SE, Bose PK, Thompson FJ, Vandenborne K. Bone loss in a new rodent model combining spinal cord injury and cast immobilization. J Musculoskelet Neuronal Interact. 2014; 14:255–266. [PubMed: 25198220]

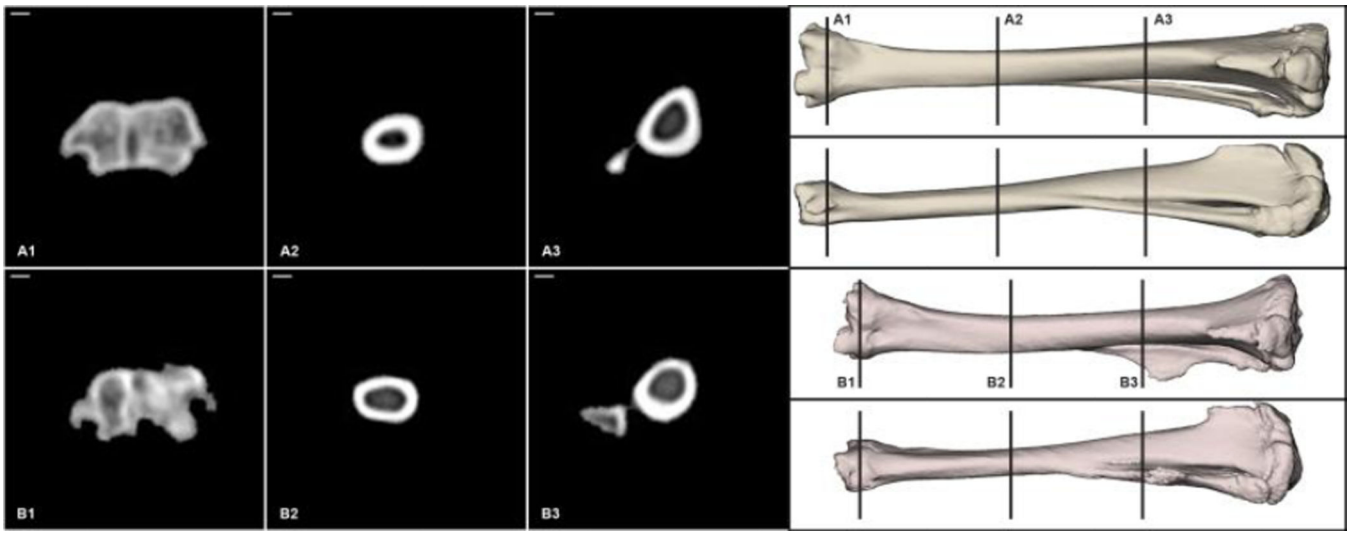

Figure 1.

Top row: healthy control rabbit tibia. Bottom row: bilateral sciatic and femoral neurectomy rabbit tibia. The 6%, 38%, and 66% total length sites are shown from left to right. Note how the bone is smaller, with spurs, and shape deformities. Note the visible thickness differences in the cortical bone.

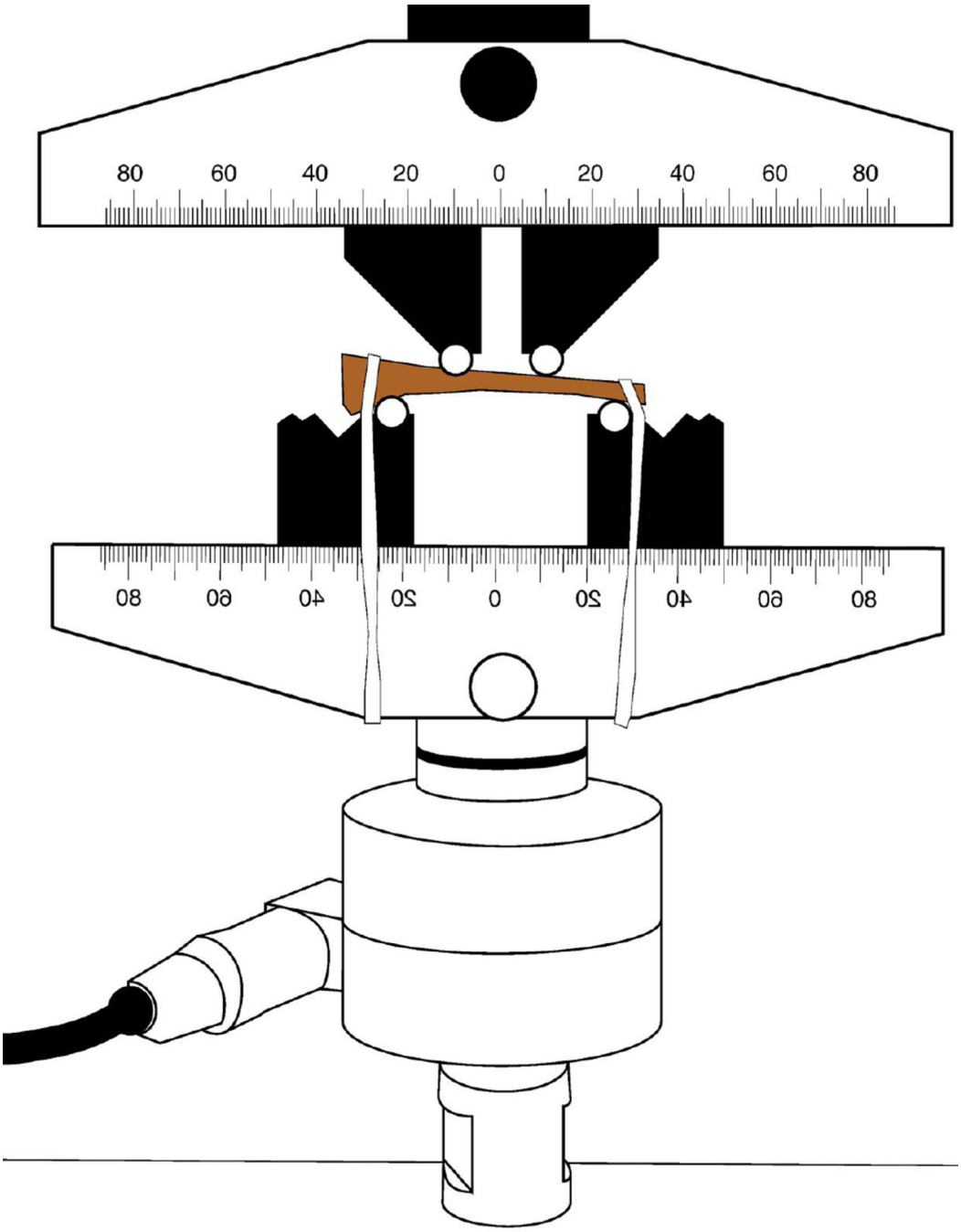

Figure 2.
Illustration depicting four-point bending experimental set-up.

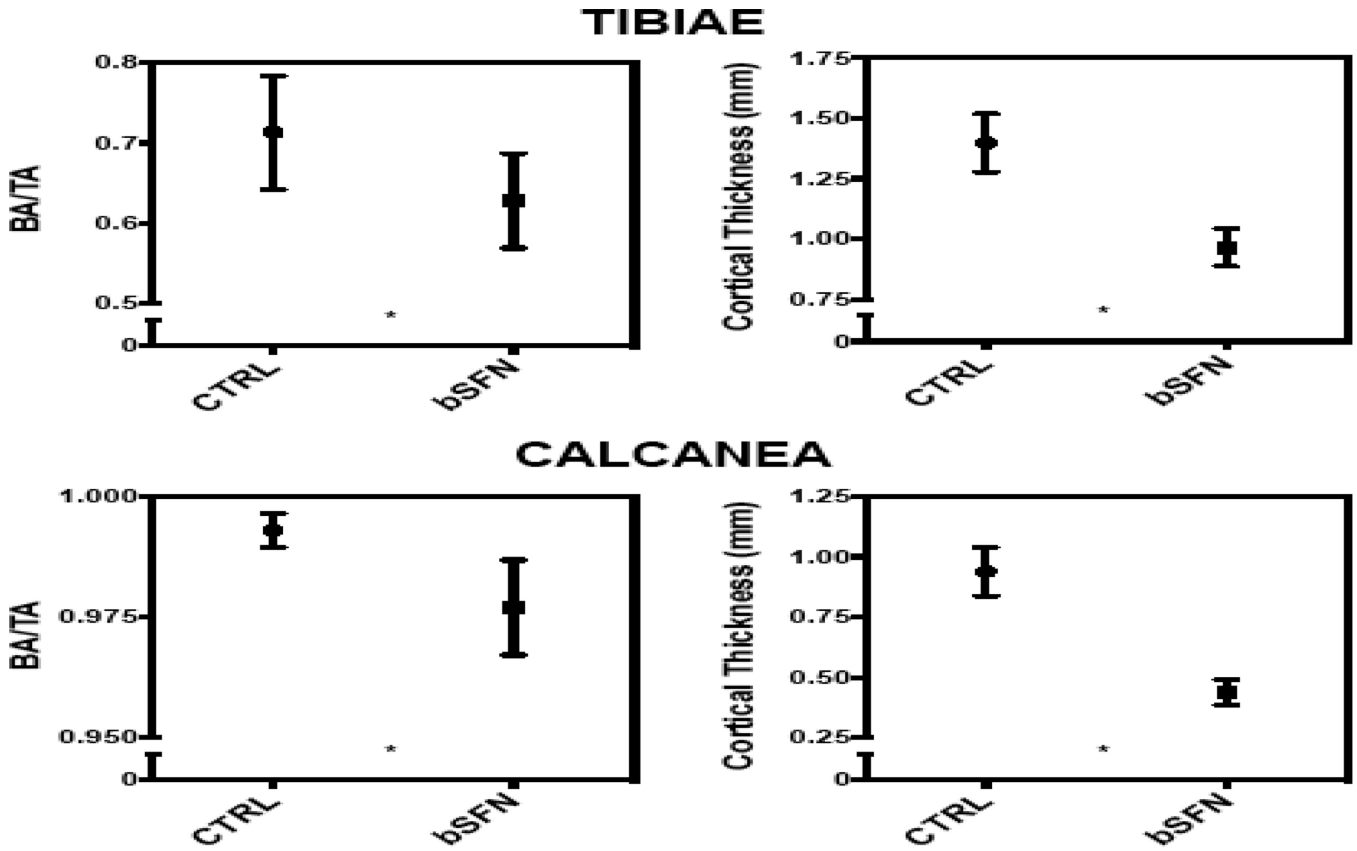

Figure 3.

Calcaneal and tibial bone area fraction and cortical thickness. The (*) denotes a significant difference between groups ($p<0.05$).

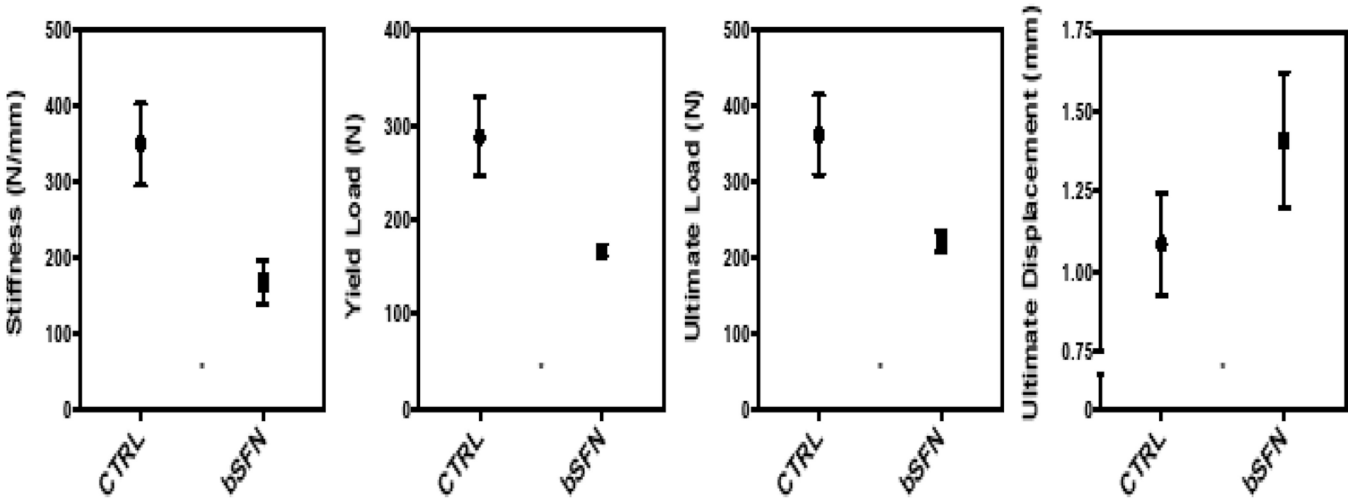

Figure 4.

Tibial bone mechanical property results. The (*) denotes a significant difference between groups ($p<0.05$).

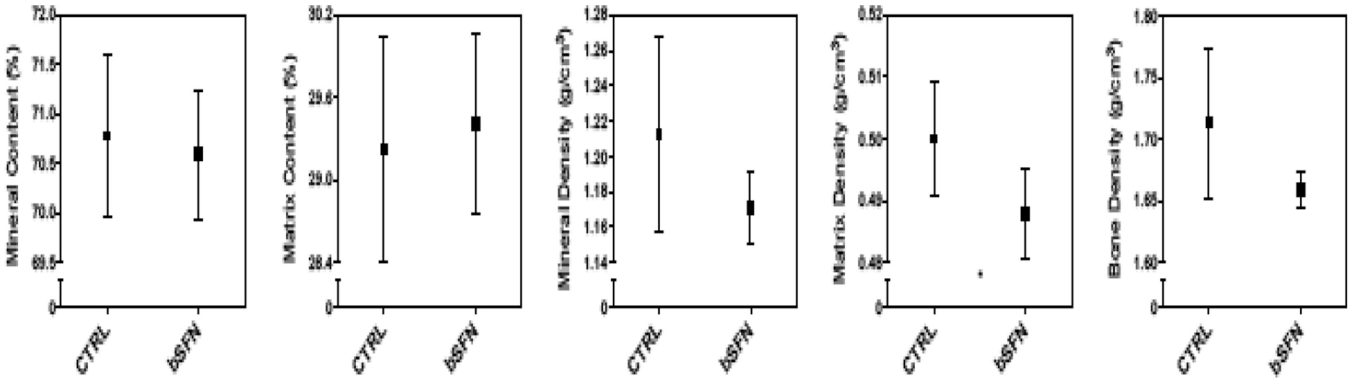

Figure 5.

True tibial bone tissue results from pycnometry. The (*) denotes a significant difference between groups ($p<0.05$).